NJC

New Journal of Chemistry

A journal for new directions in chemistry

Accepted Manuscript

This article can be cited before page numbers have been issued, to do this please use: S. Liu, K. Huang, W. Liu, Z. Meng and L. Luo, *New J. Chem.*, 2020, DOI: 10.1039/D0NJ01053G.

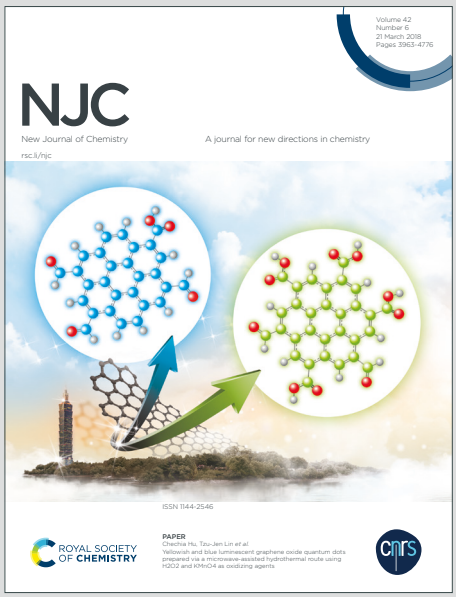

This is an Accepted Manuscript, which has been through the Royal Society of Chemistry peer review process and has been accepted for publication.

Accepted Manuscripts are published online shortly after acceptance, before technical editing, formatting and proof reading. Using this free service, authors can make their results available to the community, in citable form, before we publish the edited article. We will replace this Accepted Manuscript with the edited and formatted Advance Article as soon as it is available.

You can find more information about Accepted Manuscripts in the Information for Authors.

Please note that technical editing may introduce minor changes to the text and/or graphics, which may alter content. The journal's standard Terms & Conditions and the Ethical guidelines still apply. In no event shall the Royal Society of Chemistry be held responsible for any errors or omissions in this Accepted Manuscript or any consequences arising from the use of any information it contains.

View Article Online
DOI: 10.1039/D0NJ01053G

Cobalt-doped MoS_2 enhances the evolution of hydrogen by piezo-electric catalysis under 850 nm near-infrared light irradiation

Shou-Qing Liu*, Kuang-Zheng Huang, Wen-Xiao Liu, Ze-Da Meng, Li Luo

Jiangsu Key Laboratory of Environmental Functional Materials, School of Chemistry, Biology and Material Engineering, Suzhou University of Science and Technology, Suzhou 215009, China

* Corresponding authors, Prof. Dr. Shou-Qing Liu; Email address: shouqing_liu@163.com (S.Q.Liu); Tel:+86-512-68417050; Fax:+86-512-68415070

Abstract

Hydrogen is a clean shuttle of energy storage that can naturally reserve solar and wind energy. However, the lack of a safe and efficient storage of hydrogen in a tank for use in automobiles limits its widespread use. Therefore, developing an on-board storage and controlling the release of hydrogen are important for the practical application of hydrogen fuels. This article reported the cobalt-doped MoS_2 catalyst enhances the safe release of hydrogen from aqueous ammonia borane by piezo-photocatalysis. Results indicated that the H_2 yield of cobalt-doped MoS_2 was 4.84 times as many as that of pristine MoS_2 under ultrasonic and 850 nm near-infrared irradiation conditions. The piezo-current of the cobalt-doped MoS_2 was observed for the first time by electrochemical technique. A reaction mechanism was raised for hydrogen evolution based on an enhanced built-in field in cobalt-doped MoS_2 lattices upon piezo-electric conditions.

Keywords: Piezo-photocatalysis; Self-powered hydrogen evolution; Near-infrared irradiation; Cobalt-doped MoS_2.

View Article Online
DOI: 10.1039/D0NJ01053G

1. Introduction

Hydrogen is a clean shuttle of energy storage that can naturally reserve solar and wind energy [1]. The combustion of hydrogen gas in fuel cells in vehicles releases only clean water, which is environmental friendly and can be split into hydrogen gas by photo-catalytic, electrochemical or photo-electrochemical techniques again. However, the lack of a safe and efficient storage of hydrogen in a tank for use in automobiles limits its widespread use [2]. Therefore, developing an on-board storage and controlling the release of hydrogen are important for the practical application of hydrogen fuels. Ammonia borane (NH_3BH_3) is a leading material with high hydrogen content up to 19.6 wt.%, high stability, and non-toxicity under ambient conditions [3-7]. Thus, NH_3BH_3 is more effective and safer for storing hydrogen than gas or liquid H_2 [8,9]. In theory, hydrogen can be released from NH_3BH_3 by solvolysis or thermolysis in the presence of a suitable catalyst as follows:

$$NH_3BH_3\ (aq) + 2H_2O(l) = NH_4\ BO_2(aq) + 3H_2(g).\ \text{Eq. (1)}$$

Three moles of H_2 per mole of NH_3BH_3 can be released for fuel cells or hydrogen engines in an automobile at ambient temperature. However, the release of hydrogen from the storage material is very slow. For the fast and efficient release of hydrogen, some catalysts containing noble metals such as Pt [10,11], Pd [12], Rh [13], Au [12,14], and others [15], have been developed. Nevertheless, their applications are very limited due to the high cost and low abundance of noble metals. In the context, non-noble metal catalysts for efficient release of hydrogen need developing [16-19]. Among non-noble metal catalysts, molybdenum disulfide (MoS_2) is a suitable

View Article Online
DOI: 10.1039/D0NJ01053G

electro-catalyst and photocatalyst for hydrogen production from aqueous solution [20-22]. Some of electro-catalysts based on MoS_2 have been derived by doping [23-26], embedding [27], hybridizing [28-31], fabricating heterojunction [32-36], decorating single Ni atom on MoS_2 [37]. The piezo-catalytic performances of few-layer MoS_2, WS_2, and WSe_2 for water splitting and degradation of organic pollutants also have been reported [38]. However, the enhanced piezo-photocatalytic hydrogen production of cobalt-doped MoS_2 (Co-doped MoS_2) has not yet been reported. In the article, we described the release of hydrogen gas enhanced by doping of cobalt in MoS_2 based on piezo-electric effect and near-infrared (NIR) irradiation since MoS_2 is a conductor with narrow band gap of 1.3 eV for harvesting near-infrared irradiation.

2. Experimental section

2.1 Chemicals

Thiourea ($CS(NH_2)_2$) and cobalt chloride hexahydrate ($CoCl_2 \cdot 6H_2O$) were purchased from Sigma-Aldrich, China. Sodium molybdate dihydrate ($Na_2MoO_4 \cdot 2H_2O$) and anhydrous sodium sulfate (Na_2SO_4) were obtained from Sinopharm Chemical Reagent Co., Ltd. Ammonium borate was purchased Alddin Ltd. Indium tin oxide (ITO) conductive glass with 10 Ω was acquired from Zhuhai Kaivo Optoelectronic Technology Co. Ltd. The ITO glass was ultrasonically treated for 1 h and then dried under air conditions. All reagents used were of analytical grade and applied without further purification. All solutions were prepared with 18.2 MΩ·cm deionized Milli-Q

View Article Online
DOI: 10.1039/D0NJ01053G

water.

2.2 Synthesis of Co-doped MoS_2

$Na_2MoO_4 \cdot 2H_2O$ (2.42 g, 0.01 mol) and $(NH_2)_2CS$ (3.05 g, 0.040 mol) were separately dissolved in 30.0 mL of deionized water by vigorously stirring. $CoCl_2 \cdot 6H_2O$ (0.595 g, 0.0025 mol) was dissolved in 10.0 mL of deionized water. Then, 30.0 mL of $(NH_2)_2CS$ solution and 10.0 mL of $CoCl_2 \cdot 6H_2O$ solution were dripped in $Na_2MoO_4 \cdot 2H_2O$ solution. Deionized water of 10.0 mL was also added in the $Na_2MoO_4 \cdot 2H_2O$ solution, producing 80.0 mL of mixed solution. The mixed solution was ultrasonically dispersed for 1 h and then transferred into a 100 mL Teflon-lined stainless-steel autoclave, which was subsequently sealed and maintained at 200 °C for 24 h. The black products were collected and filtered under vacuum, washed carefully with deionized water and anhydrous ethanol in sequence, and finally dried at 60 °C in a vacuum chamber for 6 h to obtain Co-doped MoS_2 precipitates. The Co-MoS_2 sample was utilized for the characterization and piezo-photocatalytic hydrogen production. Similarly, pure MoS_2 and Co-doped MoS_2 with different doping concentrations were synthesized for comparison.

2.3 Structural Characterization

X-ray diffraction (XRD) was performed with an X'Pert-Pro MPD X-ray diffractometer (Panalytical, Netherlands). The X-ray source emitted Cu-Kα radiation with a wavelength of 0.154 nm at a tube voltage of 40 kV and a tube current of 40 mA. Morphological observations were conducted via transmission electron microscopy (TEM; Tecnai G220; FEI, USA). The Co-doped MoS_2 and MoS_2 powders were

View Article Online
DOI: 10.1039/D0NJ01053G

dispersed in water by an ultrasonication device, placed on carbon-coated copper grids, and then dried under ambient conditions prior to TEM. UV-Vis-NIR diffuse reflectance spectra (UV-Vis-NIR DRS) were recorded on a Shimadzu UV-Vis NIR spectrometer (UV-3600 plus, Japan) within the wavelength scope of 190–3400 nm. Raman spectra were obtained in LabRAM HR800 Raman analyzers.

X-ray photoelectron spectrometry (XPS) with an XSAM 800 apparatus was applied to measure the composition of the Co-doped MoS_2 catalysts and the valence states of Co, Mo, and S in the Co-doped MoS_2 with different Co-doping concentrations to reveal the piezo-catalytic and photocatalytic reaction mechanism. The carbon 1s peak at 284.60 eV was utilized to calibrate the binding energy (E_b) scale. The aluminum Ka 1.2 line (hν 1486.60 eV) worked as the X-ray excitation source, and all powder samples were dispersed on a gold-plated copper surface. To achieve maximum instrumental resolution, we recorded the spectra in fixed analyzer transmission mode. The instrument was run under a vacuum of 1×10^{-9} Torr in the analysis chamber. Wide and high-resolution spectra were recorded at a constant pass energy of 50 eV and channel widths of 1.0 and 0.1 eV.

LSV was carried out with a CHI660C electrochemistry workstation (Chen Hua Instruments, Shanghai, China) in a conventional three-electrode system, where a ITO electrode (1×1 cm^2) was utilized as the working electrode, a saturated calomel electrode (SCE) as the reference electrode, and a platinum plate as the counter electrode, respectively. All potentials were converted to the reversible hydrogen electrode (RHE). Photoelectrochemical measurements were performed in 0.50 mol/L

View Article Online
DOI: 10.1039/D0NJ01053G

H_2SO_4 solution, and a 50 W LED lamp (850 nm) was used as the NIR light source for exciting the Co-doped MoS_2 on ITO electrodes to observe the photo-currents.

Piezo-currents of the Co-doped MoS_2 were also measured with a CHI660C electrochemistry workstation as follows. First, a 10 mm × 18 mm ITO glass was used as the bottom electrode, on which about 20 mg of the Co-doped MoS_2 was uniformly distributed on a square of 10 × 10 mm^2, and then another ITO glass was used as the top electrode to fabricate a sandwich piezo-measurement cell (Fig. S1 and 2, the measurement method is reliable and believable, see Fig.S3). A swallow clincher (15 mm × 6.5 mm) was used to clamp the sandwich piezo-measurement cell to maintain its stability, and another swallow clincher was used to bring pressure on or relax the piezo-measurement cell by closing or opening it, respectively. Each of the swallow clincher exerted about 1.2 ± 0.1 kg force on the measurement cell (that is, 1.2 ± 0.1 kg force was exerted on a 10 mm × 10 mm sample when the swallow clincher was closed).

2.4 Piezo-photocatalytic hydrogen evolution

The piezo-catalytic and photocatalytic H_2 production was performed in a sealed photocatalytic reaction system (Labsolar 6A photocatalytic system, Perfect light Co. Ltd., Beijing, China) with a 100 mL aqueous solution containing 0.05 mol/L ammonium borate, which was irradiated under 50 W NIR light with λ = 850 nm. An ultrasonic generator with 200 W power was used to exert mechanical energy to the Co-doped MoS_2 for piezocatalysis at 40 KHz. It was coupled with a DC-0506 liquid thermostatic bath to maintain a constant temperature of 23 ± 2 ℃. The reaction system

View Article Online
DOI: 10.1039/D0NJ01053G

with volume of 465 mL was evacuated to the initial internal pressure at 0.01 kPa before reaction. It was matched with a GC-7806 gas chromatograph (Shiwei Puxin Instruments Co. Ltd., Beijing, China) to measure the concentration of H_2 formed during the piezo-catalytic or/and NIR photocatalytic process at 1 h intervals. A chromatographic column of 5 m length × 2 mm i.d. filled with 5 Å molecular sieve was utilized as a separating column. High-purity argon was utilized as the carrier gas. The flow rate of the carrier gas was set at 23 mL/min, and the thermal conductivity tank was used to detect H_2. The column temperature was set at 80 °C, the inlet temperature at 120 °C, and the detector temperature at 150 °C.

3 Results and discussion

3.1 Characterization of Co-doped MoS_2 nanoflowers

The as-synthesized Co-doped MoS_2 samples were observed by TEM. The flower-like Co-doped MoS_2 is displayed in Fig. 1A, where the layered structure of MoS_2 can be clearly observed. The d-spacing value of 0.63 nm in the fingerprint region of high-resolution image in Fig. 1B, which corresponds to the (002) inter-plane distance of MoS_2 crystal lattices, confirmed that the cobalt atoms were incorporated in the MoS_2 lattices. It was also confirmed by XRD as presented in Fig. 1C. The diffraction peaks of the as-synthesized MoS_2 and Co-doped MoS_2 can be indexed to the typical hexagonal structure (JCPDS 37-1492, space group: $P_3{}^6$/mmc, a = 3.12 Å, c = 12.555 Å, α = β = 90° and γ = 120°) of crystalline MoS_2 [39]. Four diffraction peaks at 2θ = 13.3°, 35.8°, 39.5°, and 57.6° were assigned to the Bragg diffractions from the

View Article Online
DOI: 10.1039/D0NJ01053G

(002), (100), (103), and (110) planes of MoS_2, respectively. In particular, the primary peak for both samples at 2θ = 13.3°, which corresponds to the (002) diffraction plane of MoS_2, together with the d-spacing of 0.63 nm in Fig. 1B, confirmed that cobalt atoms were doped in MoS_2 lattice structure.

The typical photoluminescence spectrum of Co-doped MoS_2 nanoflowers is depicted in Fig. 1D, displaying broad emission in the wavelength scope of 360–800 nm. The broad PL spectrum was deconvoluted into three separate peaks using Gaussian fitting as shown in Fig. 1E. An intense peak centered at 525 nm (2.36 eV) is attributed to the emission from Co-doped MoS_2 nanocrystals, which is in very good agreement with the absorption peak of MoS_2 in the UV-Visible NIR diffuse reflectance spectra (UV-Vis-NIR DRS) in Fig. 2A, whereas the weak transitions centered at 640 (1.94 eV) and 720 nm (1.72 eV) are the characteristic emission peaks of few-layer Co-doped MoS_2 [40], which correspond to the direct band gaps of the as-synthesized Co-doped MoS_2. The split valence band (220 meV) between two weak transitions may be related to the incorporation of cobalt atoms into MoS_2 lattices.

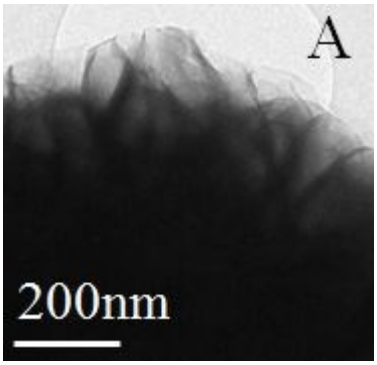

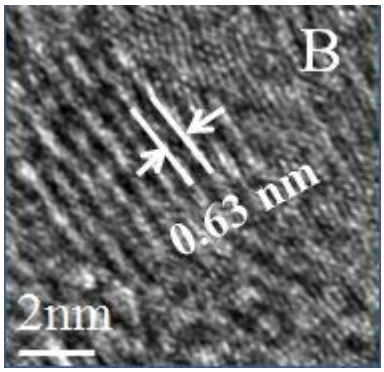

View Article Online
DOI: 10.1039/D0NJ01053G

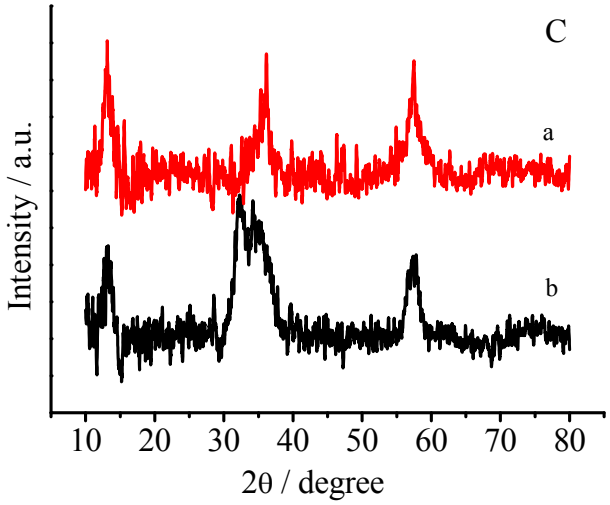

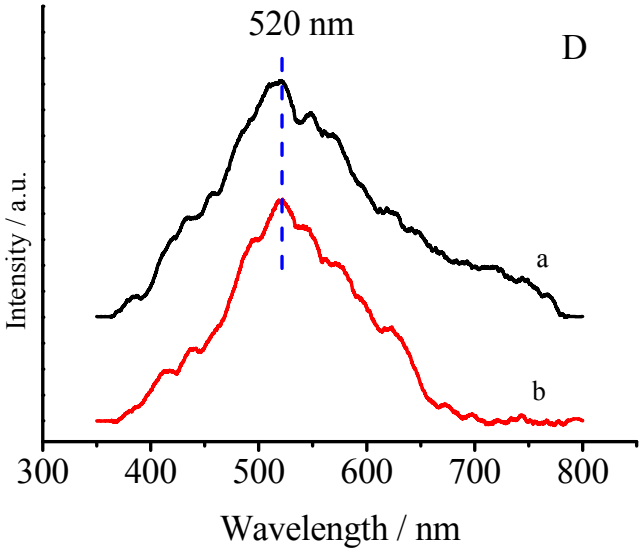

View Article Online
DOI: 10.1039/D0NJ01053G

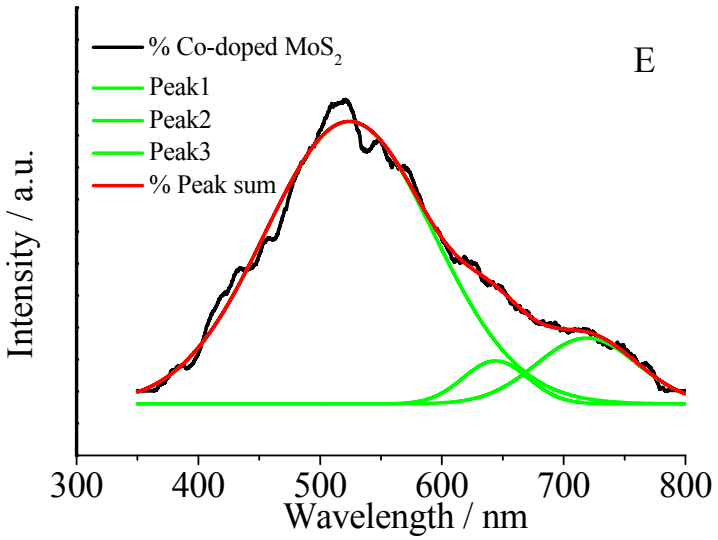

Fig. 1. (A) TEM image of the as-synthesized Co-doped MoS_2 nanoflowers. (B) high-resolution TEM image of Co-doped MoS_2 with 0.63 nm spacing-d value. (C) XRD patterns of the as-synthesized Co-doped MoS_2 (a) and MoS_2 (b) nanoflowers. (D) PL emission spectra of Co-doped MoS_2 (a) and MoS_2 (b) nanoflowers exited by 325 nm laser. (E) Deconvoluted PL emission spectrum of Co-doped MoS_2.

UV-Visible NIR diffuse reflectance spectra in Fig. 2A indicate an absorption peak at 895 nm both in MoS_2 and Co-doped MoS_2 samples, revealing an absorption response to NIR irradiation. Simultaneously, a blue-shift occurred in the visible region after cobalt atoms were incorporated in MoS_2 lattices as shown in curve (a) in Fig. 2A. The UV-Visible NIR diffuse reflectance curves were transmitted, and $(ahv)^{1/2}$ was plotted against photon energy hv in terms of Tauc formula, thereby forming curves (a) and (b) in Fig. 2B. The linear relation of $(ahv)^{1/2}$ against hv demonstrated the indirect transition of carriers excited by photons in the materials. The resulting intercept was 0.96 eV in the case of Co-doped MoS_2, which is 0.04 eV

View Article Online
DOI: 10.1039/D0NJ01053G

smaller than that in the case of pristine MoS_2. In general, the indirect band gap of MoS_2 is 1.30 eV. The small band gaps might be caused by the lower crystallinity and defects in the synthesized MoS_2. An increase in defect degree will lead to narrowing of the band gap [41-43].

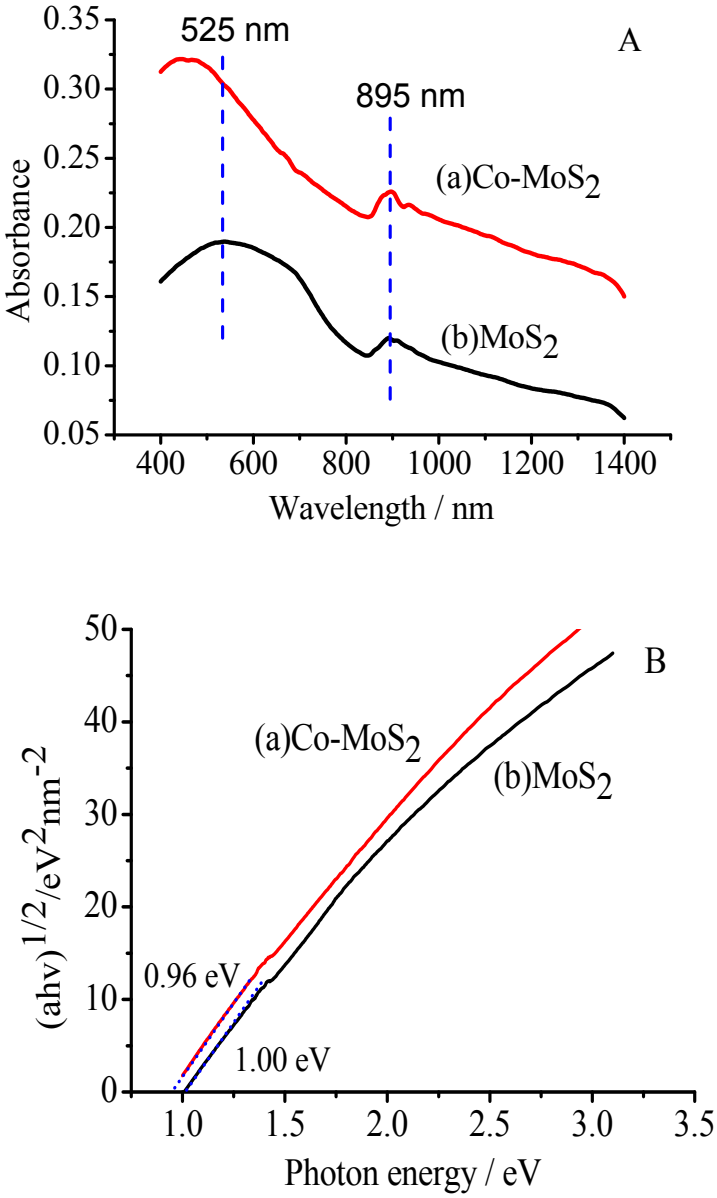

Fig. 2 (A) UV-Vis-NIR DRS of the as-synthesized Co-doped MoS_2 (a) and MoS_2 (b) samples. (B) Tauc plots for the indirect band gaps of Co-doped MoS_2 (a) and MoS_2 (b) samples.

View Article Online
DOI: 10.1039/D0NJ01053G

The composition of the as-synthesized Co-doped MoS_2 material was further explored by X-ray photoelectron spectroscopy (XPS). The XPS survey spectrum indicated the presence of molybdenum, sulfur, cobalt, and oxygen in the Co-doped MoS_2, whereas no cobalt was found in undoped MoS_2 (Fig. 3A). The binding energies located at 229.0 and 232.6 eV were attributed to 3d5/2 and 3d3/2 of Mo(IV), respectively, and the shoulder peak at 226.0 eV corresponded to the binding energy of S 2p (Fig.3B). The peaks at 232.0 and 236.0 eV revealed a fraction of Mo(VI) in the as-synthesized Co-doped MoS_2, showing that Mo(VI) was not completely reduced to Mo(IV) during the hydrothermal reaction. A fraction of MoO_3 was possibly present in the as-synthesized species because oxygen was also detected in the XPS survey spectra [44,45]. On the basis of the high-resolution S 2p spectrum in Fig. 3C, the doublet peaks located at 161.7 and 162.9 eV were assigned to the 2p 3/2 and 2p 1/2 of S^{2-} in the Co-doped MoS_2, whereas the peak located at 169.2 eV was ascribed to S^{6+} [45]. The Co 2p spectra were fitted with four doublets (Fig. 3D). A pair of peaks at 779.1 and 793.9 eV with a wide separation of 14.8 eV because of the strong spin orbit coupling (14.8 eV) of the Co 2p peak were from 2p 3/2 and 2p 1/2 of Co^{2+} in the Co-doped MoS_2 phase, respectively, whereas the other ones at 782.0 and 797.9 eV were from 2p 3/2 and 2p 1/2 of Co^{2+}. It may originate from the presence of $CoSO_4$ because the peak of S^{6+}, as shown previously, was found in Fig.3C [45,46].

View Article Online
DOI: 10.1039/D0NJ01053G

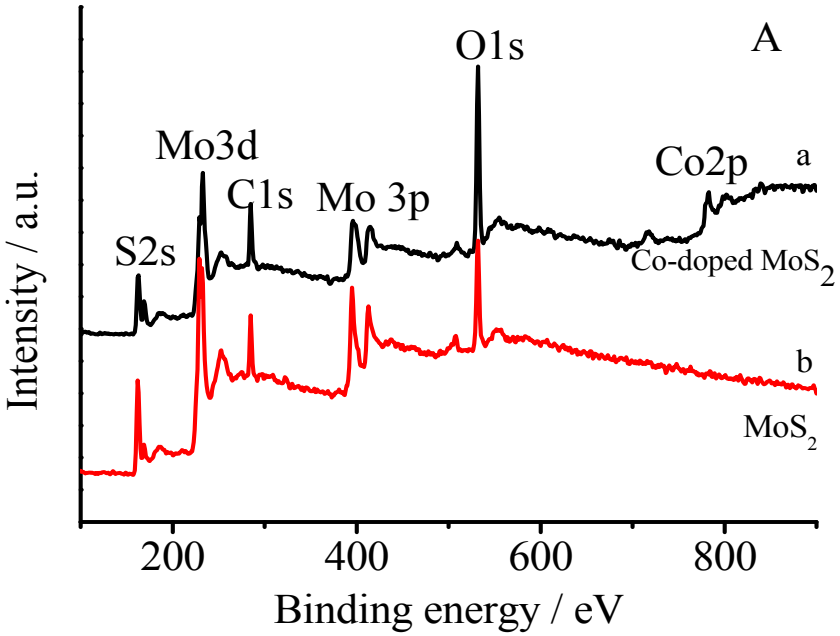

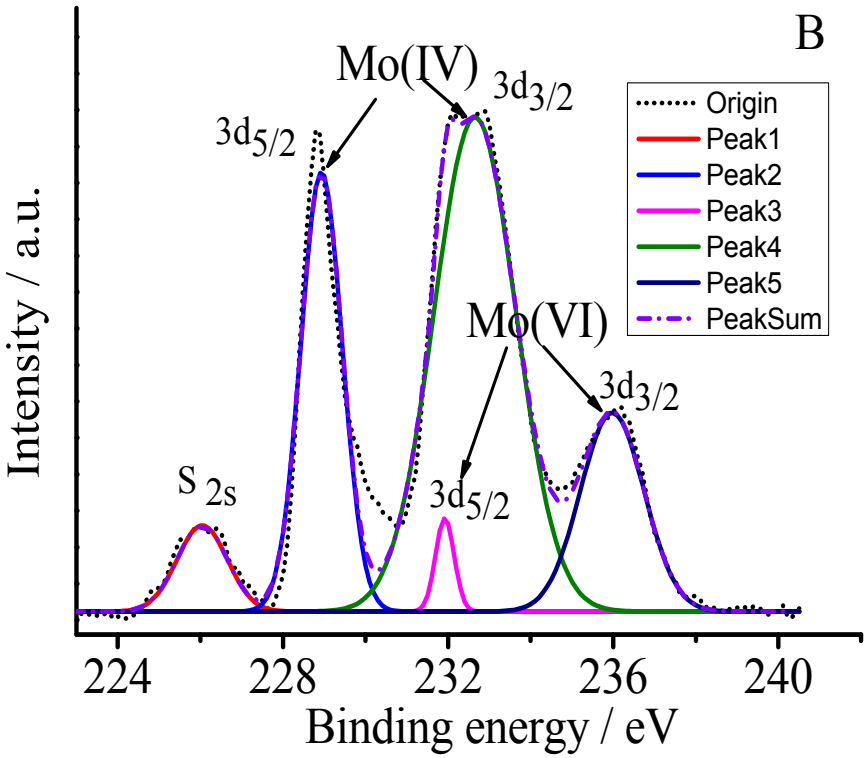

View Article Online
DOI: 10.1039/D0NJ01053G

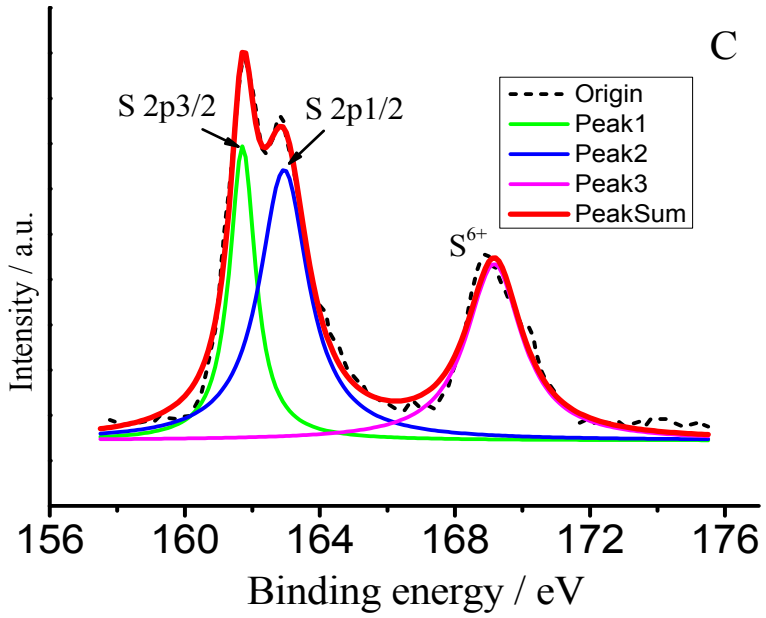

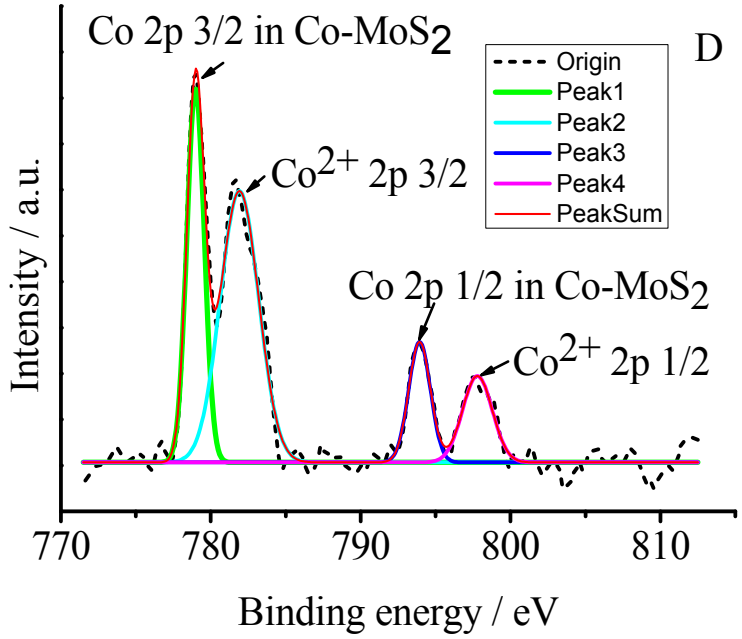

Fig. 3. (A) XPS survey spectra of Co-doped MoS_2 and undoped MoS_2. (B) High-resolution Mo 3d XPS spectra. (C) High-resolution S 2p XPS spectra. (D) High-resolution Co 2p XPS spectrum.

View Article Online
DOI: 10.1039/D0NJ01053G

3.2 Hydrogen yield enhanced by doping of cobalt under ultrasonic and 850 nm NIR irradiation

The pristine MoS_2 and a series of Co-doped MoS_2 samples were synthesized to compare with their piezo-photocatalytic activities as shown in Fig.4. The results indicated that the yield of hydrogen was boosting with the content of cobalt doped in MoS_2 as presented in curves b, c, d, e, compared with curve a in pristine MoS_2. **The top value approached to 1.84 mmol H_2 when the cobalt content reached 12.78%, which is 4.8-fold as many as that in pristine MoS_2 (0.38 mmol) under similar conditions**. It showed that the doping of cobalt significantly enhanced the piezo-photocatalytic activity of MoS_2, which is similar to the doping of vanadium in $BiOIO_3$ [47], also, to the replacement of halogen ions for OH in $Bi_2O_2(OH)(NO_3)$[48]. Instead, the yield of hydrogen started to decrease as shown in curves g and h when the content of cobalt exceeded 12.8%, indicating an optimum content of cobalt doped in MoS_2.

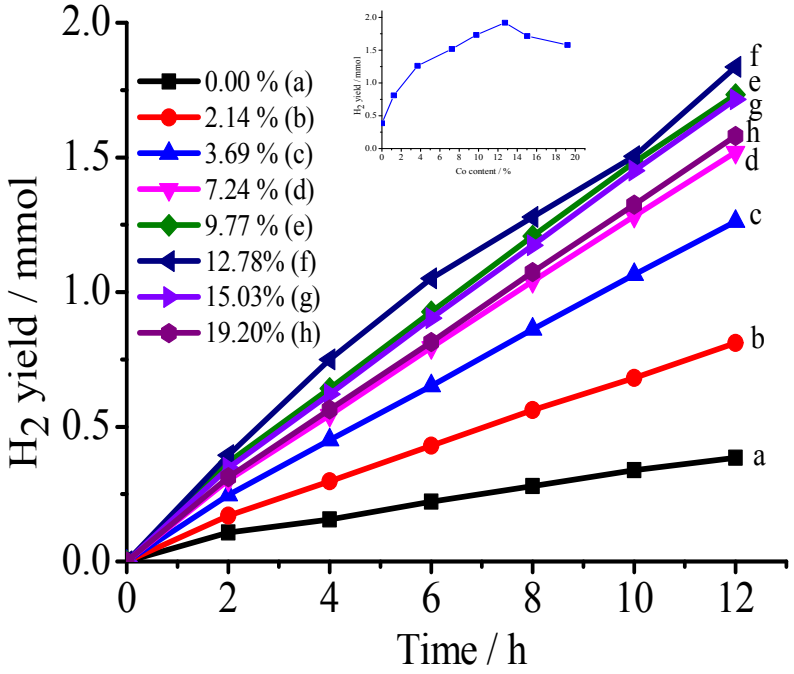

View Article Online
DOI: 10.1039/D0NJ01053G

Fig. 4. Effects of doping of cobalt in MoS_2 on hydrogen yield. The evolution of hydrogen using 0.10 g of MoS_2 as catalyst in 0.05 mol/L NH_3BH_3 100 mL solution under ultrasonic and 850 nm irradiation conditions. The content of cobalt doped in MoS_2: (a), 0.00% (pristine MoS_2); (b), 2.14%; (c), 3.69%; (d), 7.24%; (e), 9.77%; (f), 12.78%; (g), 15.03; (h), 19.20%.

In order to survey the effects of the ultrasonic, irradiation and Co-doped MoS_2, respectively, the blank and control tests were done. The results revealed that 0.24 mmol hydrogen was turned out naturally without catalyst, ultrasonic vibration nor NIR irradiation as shown in curve 1 in Fig.5. The hydrogen yield rose to 0.62 mmol (curve 2) when 0.10 g of Co-doped MoS_2 catalyst was used in 0.05 mol/L NH_3BH_3 100 mL solution even without ultrasonic vibration nor NIR irradiation, indicating the Co-doped is capable of promoting hydrogen generation. The NH_3BH_3 solution containing 0.1 g Co-doped MoS_2 catalyst was irradiation only by 850 nm NIR, producing 0.84 mmol hydrogen gas (curve 3). The same solution containing 0.1 g Co-doped MoS_2 catalyst was excited only by ultrasonic wave, resulting in 0.92 mmol hydrogen (curve 4). The yield of 0.92 mmol is larger than that of 0.62 mmol in the presence of the catalyst but absence of ultrasonic wave as shown in curve 2, revealing ultrasonic wave significantly fastening the formation of hydrogen. Moreover, the hydrogen yield raised to 1.84 mmol under similar conditions when ultrasonic and NIR irradiation were applied simultaneously (curve 5). These data are listed in Table 1.

View Article Online
DOI: 10.1039/D0NJ01053G

Table 1. Yields of hydrogen gas under different conditions

No.	Catalyst	Irradiation	Ultrasonic	Yield / mmol	*Elevated yield / mmol
1	No	No	No	0.24	/
2	Yes	No	No	0.62	0.00
3	Yes	Yes	No	0.84	0.22
4	Yes	No	Yes	0.92	0.30
5	Yes	Yes	Yes	1.84	1.22

*Elevated yield is defined as the difference between the corresponding hydrogen yield and one that only in the presence of 0.1 g Co-doped MoS_2 without irradiation nor ultrasonic vibration.

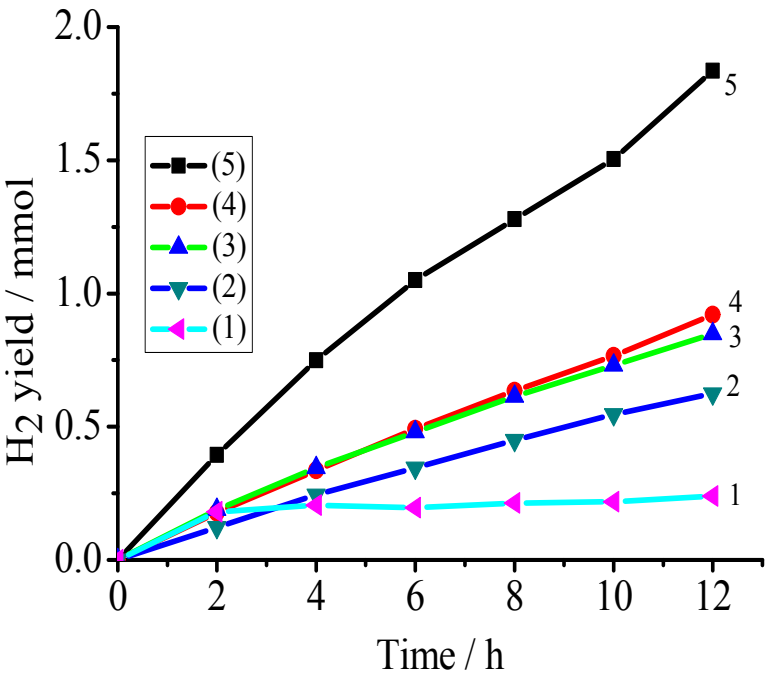

Fig. 5. Blank and control tests. (1), natural hydrogen yield of 0.05 mol/L NH_3BH_3 100 mL solution without catalyst, ultrasonic vibration nor NIR irradiation; (2), 0.10 g of Co-doped MoS_2 catalyst in 0.05 mol/L NH_3BH_3 100 mL solution without

View Article Online
DOI: 10.1039/D0NJ01053G

ultrasonic vibration and NIR irradiation; (3), in the case of (2) only upon 850 nm NIR irradiation; (4), in the case of (2) excited only by ultrasonic vibration; and (5),in the case of (2) excited by both ultrasonic vibration and NIR irradiation.

Compared with curve 2 in the case of Co-doped MoS_2 catalyst, curve 3 demonstrated an elevated hydrogen yield (0.22 mmol) under NIR irradiation, implying that Co-doped MoS_2 is capable of harvesting NIR energy. Moreover, the elevated hydrogen yield (0.3 mmol) under ultrasonic vibration is higher than that under NIR irradiation, indicating that ultrasonic energy improved more efficiently the yield. Most of all, the elevated yield approached to 1.22 mmol under both ultrasonic and NIR irradiation, which is still larger than the sum (0.52 mmol) of ultrasonic and NIR irradiation, indicating the synergism between the ultrasonic and NIR irradiation. In addition, the control experiment using 0.1 g Co-doped MoS_2 catalyst in water with ultrasonic vibration and without NH_3BH_3. The results showed the 25.5 nmol H_2 was detected at 12 h, this value is much less than 1.22 mmol (1.22×10^6 nmol), which is the case in the presence of 0.1 g Co-doped MoS_2 catalyst in 0.05 mol/L NH_3BH_3 100 mL solution excited by both ultrasonic vibration and NIR irradiation. Also, the 25.5 nmol H_2 is less than that (0.3 mmol) in the case in the presence of 0.1 g Co-doped MoS_2 catalyst in 0.05 mol/L NH_3BH_3 100 mL solution excited only by ultrasonic vibration. The recycling tests with 0.1 g Co-doped MoS_2 on the hydrogen evolution have been conducted for 5 runs under piezo-photo-catalytic conditions. The results showed that the yield still maintained about 1.83 mmol even at 5th run, indicating the Co-doped MoS_2 catalyst is very stable.

3.3 Mechanism exploration

3.3.1 Evidences for piezo-electric effect and NIR response

In order to confirm the piezo-electric effect, the piezo-currents of the Co-doped

View Article Online
DOI: 10.1039/D0NJ01053G

MoS_2 and pristine MoS_2 were measured by exerting a pressure of 1.1 ± 0.1 kg/cm^2 on between ITO electrodes, respectively, the results were shown in Fig. 6 (the detailed procedures could be in Supplementary Materials).

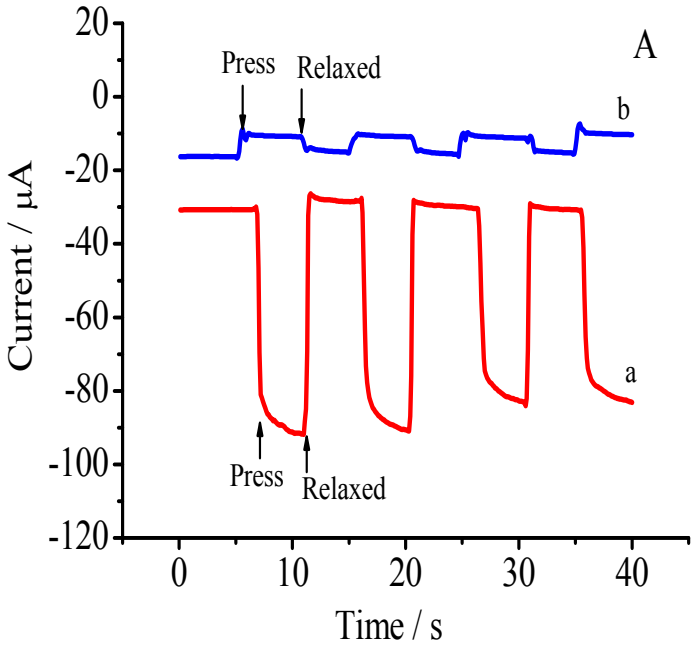

Fig. 6. Piezo-current signals measured by the i-t curve technique for applied pressure. The potential of the top electrode was set as 0.00 V *versus* reference or working electrode. (a) Co-doped MoS_2. (b) pristine MoS_2.

The remarkable piezo-currents of both Co-doped MoS_2 and pristine MoS_2 were observed. The piezo-current derived from the Co-doped MoS_2 is about -60 μA/cm^2, whereas the one derived from pristine MoS_2 is about 8 μA/cm^2. By comparison, the absolute value of the piezo-current derived from the Co-doped MoS_2 is nearly 8 times as much as that of the piezo-current from pristine MoS_2, which is in good agreement with the hydrogen yield. Thus, the enhanced piezo-catalytic activity is attributed to the doping of cobalt in MoS_2.

It is known well that the piezoelectric effect is a coupling of mechanics and

electric polarization. When a dielectric material is deformed through an applied force along its asymmetry direction, the positive and negative charges are generated on two opposite surfaces. The asymmetry of the material will facilitate its electric polarization, resulting in enhancing the built-in electric field. In turn, the enhanced built-in electric field will promote the separation of charges generated on irradiation. In our case, the doping of cobalt in MoS_2 increased its asymmetry in structure, resulting in enhanced piezoelectric effect [47,48]. The enhanced piezoelectric effect fabricated a polar built-in electric field, facilitating the more efficient separation of photo-generated carries and increasing the hydrogen yield.

In order to elucidate the role of NIR irradiation, the linear sweep voltammetry was used to detect the currents of Co-doped MoS_2 upon NIR irradiation and in the dark as shown in Fig.7, respectively.

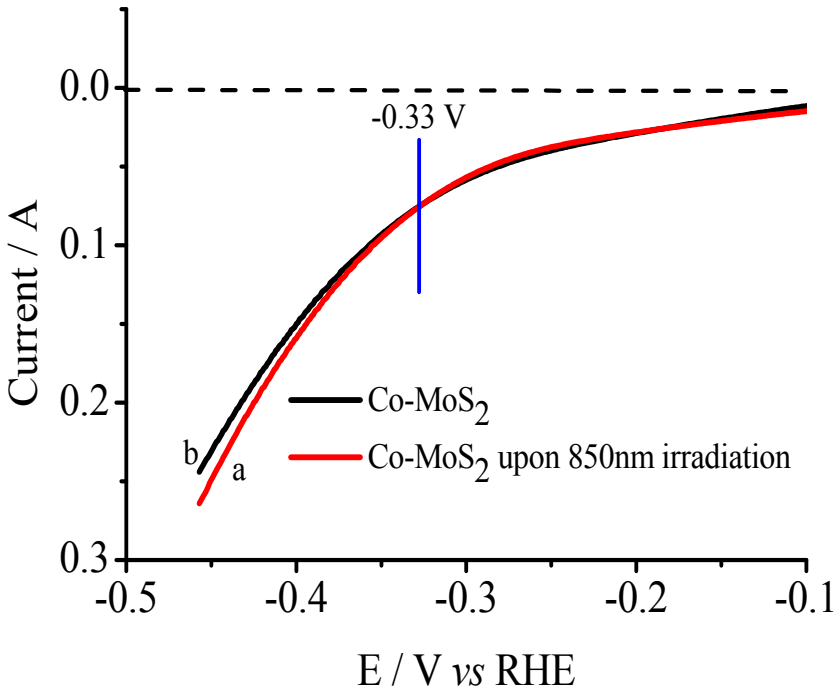

Fig. 7. Linear sweep voltammetric curves of Co-doped MoS_2 on ITO electrode in 0.50 mol/L H_2SO_4 solution upon 850 nm NIR irradiation (a) and in the dark (b). Sweep rate was 5.0 mV/s.

View Article Online
DOI: 10.1039/D0NJ01053G

Compared with the dark current, the photo-current start to appear at -0.33 V vs RHE upon NIR irradiation, which revealed the Co-doped MoS_2 material is capable of transforming NIR irradiation to electric energy. It is reasonable that the indirect band gap of MoS_2 falls in the range of 1.16–1.30 eV [49-51], which indicated that the material can harvest NIR irradiation to produce hydrogen gas.

3.3.2 Reaction mechanism

Piezoelectrics can produce polarized positive charges (+) on one end of the unit and negative charges (-) on the other end under either stress or strain. Driven by piezoelectric polarization field, the photoinduced e^- and h^+ can be efficiently separated and propelled to migrate in opposite directions, benefiting the migration of bulk charges to surface active sites for participating in various photocatalytic reactions [48,52,53]. It has been known that Co-doped MoS_2 possesses both piezo-electric property and photo-electric transformation property based on the piezo-currents and photo-currents mentioned above. Thus, a built-in electric field in lattices of Co-doped MoS_2 can be fabricated upon oscillation, as shown in Fig.8. Then, the positive and negative photo-generated carries are generated under NIR irradiation. Finally, the photo-generated positive charges migrate along the direction of the built-in electric field and the photo-generated negative charges shift opposite to the direction of the built-in electric field. As a result, the hydrogen gas is formed fast. The overall reaction mechanism could be displayed in Fig. 8.

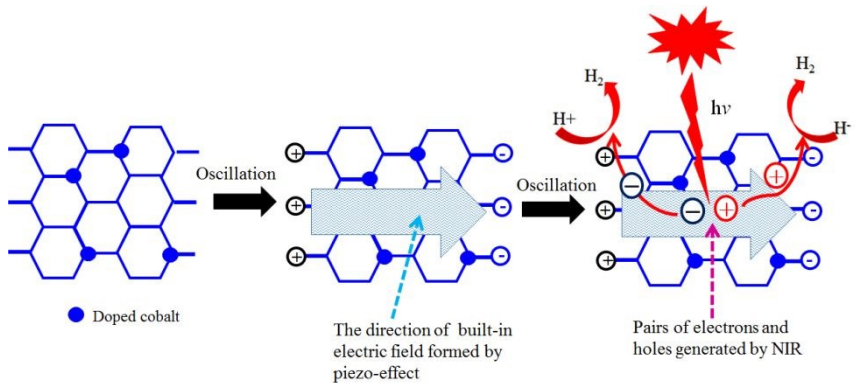

Fig. 8. Reaction mechanism of piezo-photocatalytic H_2 production of Co-doped MoS_2

View Article Online
DOI: 10.1039/D0NJ01053G

Conclusion

The doping of cobalt in MoS_2 enhanced the piezo-electricity of MoS_2, which fabricated a stronger built-in electric field in lattices of Co-doped MoS_2. It, in turn, promoted the separation of photo-generated electrons and holes, and resulted in a high yield of hydrogen. The enhanced piezo-catalytic feature of Co-doped MoS_2 for H_2 evolution could be regarded as a self-powered model of hydrogen evolution for vehicles due to vehicle vibration on run.

Conflicts of interest

There are no conflicts to declare.

Acknowledgments

This work is financially supported by the National Natural Science Foundation of China (No.21576175), and Collaborative Innovation Center of Technology and Material of Water Treatment.

References

1 X. Yu, X. Han, Z. Zhao, J. Zhang, W. Guo, C. Pan, A. Lia, H. Liu and Z. L. Wang, *Nano Energy*, 2015,11, 19–27.

2 T. B. Marder, *Angew. Chem. Int. Ed.*, 2007, 46, 8116 – 8118.

3 S. Akbayrak and S. Özkar, *Int. J. Hydrogen Energy*, 2018, 43, 18592-18606.

4 A. Rossin and M. Peruzzini, *Chem. Rev.*, 2016, 116, 8848−8872.

5 S. Bhunya, T. Malakar, G. Ganguly and A. Paul, *ACS Catal.*,2016, 6, 7907−7934.

View Article Online
DOI: 10.1039/D0NJ01053G

6 N.C.Smythe and J.C. Gordon, *Eur. J. Inorg. Chem*., 2010, 509-521.

7 B. Peng and J. Chen, *Energy Environ. Sci.,* 2008,1, 479-483.

8 N.L. Rosi, *Science*, 2003, 300, 1127-1129.

9 P. Chen, Z. Xiong, J. Luo, J. Lin and K.L. Tan, *Nature,* 2002, 420,302-304.

10 F. Fu, C. Wang, Q. Wang, A. M. Martinez-Villacorta, A. Escobar, H. Chong, X. Wang, S. Moya, L. Salmon, E. Fouquet, J. Ruiz and D. Astruc, *J. Am. Chem. Soc.,* 2018,140, 10034−10042.

11 M. A. Khalily, H. Eren, S. Akbayrak, H. H. Susapto, N. Biyikli, S. Zkar and M. O. Guler, *Angew. Chem. Int. Ed.*, 2016,128, 1 – 6.

12 S. Rej, C. F. Hsia, T. Y. Chen, F. C. Lin, J. S. Huang and M. H. Huang, *Angew. Chem. Int. Ed.*, 2016, 55, 7222 –7226.

13 D. Özhava and S. Özkar, *Applied Catalysis B: Environ.*, 2018, 237,1012-1020.

14 J.M. Yan, X.B. Zhang, T.Akita, M. Haruta and Q. Xu, *J. Am. Chem. Soc.*, 2010, 132,5326–5327.

15 W.W. Zhan, Q.L. Zhu and Q. Xu, *ACS Catal.*,2016, 6, 6892−6905.

16 C. Wang, J. Tuninetti, Z.Wang, C. Zhang, R. Ciganda, L. Salmon, S. Moya, J. Ruiz and D. Astruc, *J. Am. Chem. Soc.*, 2017,139, 11610−11615.

17 X. Zhou, X.F. Meng, J.M. Wang, N. Z. Shang, T. Feng, Z. Y. Gao, H.X. Zhang, X.L. Ding, S.T. Gao, C. Feng and C. Wang, *Int. J. Hydrogen Energy*, 2019, 44, 4764-4770.

18 K. Feng, J. Zhong, B. Zhao, H. Zhang, L. Xu, X. Sun and S.T. Lee, *Angew. Chem. Int. Ed.*, 2016,55, 11950-11954.

19 Z.Tang, H. Chen, X. Chen, L. Wu and X. Yu, *J. Am. Chem. Soc.*, 2012,134, 5464−5467.

20 H. I. Karunadasa, E. Montalvo, Y. Sun, M. Majda, J. R. Long and C. J. Chang, *Science*, 2012, 335(6069), 698-702.

21 Y. Wang, Z. Wang, Q. Yang, A. Hua, S. Ma, Z. Zhang and M. Dong, *New J. Chem.*, 2019,43, 6146-6152.

22 M.Yin, W. Zhang, H. Li, C. Wu, F. Jia, Y. Fan and Z. Li, *New J. Chem.*, 2019,43, 1230-1237.

23 T. Sun, J. Wang, X. Chi, Y. Lin, Z. Chen, X. Ling, C.Qiu, Y. Xu, L.Song, W. Chen and C. Su, *ACS Catal.,* 2018, 8,7585–7592.

24 Q. Xiong, Y. Wang, P.F. Liu, L. R. Zheng, G.Wang, H.G. Yang, P.K. Wong, H. Zhang and H. Zhao, Adv. Mater.,2018, 30,1801450.

25 Q. Xiong, X. Zhang, H. Wang, G. Liu, G. Wang, H. Zhang and H. Zhao, *Chem. Commun.,*2018, 54, 3859-3862.

26 Y.Li, J. Wang, X. Tian, L. Ma, C. Dai, C. Yang and Z. Zhou, *Nanoscale*, 2016, 8, 1676-1683.

27 H. Lee, D. A. Reddy, D. P. Kumar, M. Lim and T. K. Kim, *Appl. Surf. Sci.,*2019, 494, 239 – 248

28 X. Zhao, Y. Li, Y. Guo, Y. Chen, Z. Su and P. Zhang, *Adv. Mater. Interfaces*,2016, 3, 1600658.

29 S. Das, R. Ghosh, P. Routh, A. Shit, S. Mondal, A.Panja and A. K. Nandi, *ACS Appl. Nano Mater.,*2018, 1, 2306–2316.

30 D. Escalera-López, Y. Niu, J. Yin, K. Cooke, N. V. Rees and R. E. Palmer, *ACS Catal.*,2016, 6, 6008–6017.

31 W. Ma, H. Li, S. Jiang, G. Han, J. Gao, X. Yu, H. Lian, W.Tu, Y. Han and R. Ma, *ACS Sustainable Chem. Eng.,*2018, 6, 14441–14449.

32 Y. Zhu, L. Song, N. Song, M. Li, C.Wang and X. Lu, *ACS Sustainable Chem. Eng*.,2019, 7, 2899–2905.

33 D. Vikraman, S. Hussain, K. Akbar, L. Truong, A. Kathalingam, S.H. Chun, J. Jung, H. J. Park and H.S. Kim, *ACS Sustainable Chem. Eng.*,2018, 6,8400–8409.

34 C. Du, D. Liang, M. Shang, J. Zhang, J. Mao, P. Liu and W. Song, *ACS Sustainable Chem. Eng.,*2018, 6, 15471–15479.

35 L.X. Chen, Z.W. Chen, Y. Wang, C. C. Yang and Q. Jiang, *ACS Catal.,*2018, 8, 8107–8114.

36 Z. Wu, J. Wang, K. Xia, W. Lei, X. Liu and D. Wang, *J. Mater. Chem. A*, 2018,6,616-622.

37 Q. Wang, Z. L. Zhao, S. Dong, D. He, M. J. Lawrence, S. Han, C. Cai, S. Xiang, P. Rodriguez, B. Xiang, Z. Wang, Y. Liang and M. Gu, Nano Energy, 2018,53, 458-467.

38 S. Li, Z. Zhao, D. Yu, J. Zhao, Y. Su, Y. Liu, Y. Lin, W. Liu, H. Xu and Z. Zhang, Nano Energy, 2019,66, 104083.

39 J. H. Lin, Y.H. Tsao, M.H. Wu, T.M. Chou, Z.H. Lin and J. M. Wu, *Nano Energy,* 2017, 31, 575 – 581.

40 S. Mukherjee,R. Maiti, A. Midya, S. Das and S.K. Ray, *ACS Photonics*, 2015, 2, 760−768.

View Article Online
DOI: 10.1039/D0NJ01053G

41 K. K.Kam and B. A.Parkinson, *J. Phys. Chem.*,1982, 86, 463 – 467.

42 X. B.Chen, L. Liu, P. Y. Yu and S. S.Mao, *Science*, 2011, 331, 746 – 750.

43 K. Chang, Z. Mei, T. Wang, Q. Kang, S. Ouyang and J. Ye, *ACS Nano*,2014, 8, 7078 – 7087.

44 J. D.Benck, Z.B. Chen, L.Y. Kuritzky, A.J. Forman and T. F. Jaramillo, *ACS Catal.*,2012, 2, 1916−1923.

45 X. Dai, K. Du, Z. Li, M. Liu,Y. Ma, H. Sun, X. Zhang and Y. Yang, *ACS Appl. Mater. Interfaces,*2015, 7, 27242−27253.

46 R. Bose, Z. Jin, S. Shin, S. Kim, S. Lee and Y.S. Min, *Langmuir*, 2017, 33, 5628−5635.

47. H. Huang,S. Tu,C. Zeng,T. Zhang,A. H. Reshak and Y. Zhang, *Angew. Chem. Int. Ed.,* 2017, 56, 11860-11864.

48. L.Hao,L. Kang,L. Ye,K. Han,S. Yang,H. Yu,M. Batmunkh and Y. Zhang,T. Ma, *Adv. Mater.*, 2019, 31, 1900546.

49 Z. Li, G. Ezhilarasu, I. Chatzakis, R. Dhall, C.C.Chen and S. B. Cronin， *Nano Lett*., 2015, 15, 3977–3982.

50 Z. Wang, Q. Chen and J. Wang，*J. Phys. Chem. C,* 2015, 119,4752−4758.

51 B. Cao and T. Li, *J. Phys. Chem. C*,2015, 119, 1247−1252.

52 F. Chen, H. Huang, L. Guo, Y. Zhang and T. Ma, *Angew. Chem. Int. Ed.,* 2019, 131, 10164 – 10176.

53 C.Hu, H. Huang, F.g Chen, Y.Zhang, H. Yu, and T.Ma, *Adv. Funct. Mater.,* 2020, 30, 1908168.